Continuation Three-Phase Power Flow: A Tool for Voltage Stability Analysis of Unbalanced Three-Phase Power Systems

Xiao-Ping Zhang, *Member, IEEE*, Ping Ju, *Member, IEEE*, and Edmund Handschin, *Fellow, IEEE*

***Abstract*—In this paper, a continuation three-phase power flow (CTPFlow) approach in polar coordinates, which can be used to analyze voltage stability of unbalanced three-phase power systems, is proposed. Using CTPFlow, the PV curves of unbalanced three-phase power systems can be obtained. It is found that the patterns of the PV Curves of unbalanced three-phase power systems are quite different from that of balanced three-phase power systems or positive-sequence power systems. The investigations indicate that a CTPFlow is needed where there are unbalanced network or loads existing in a system. Numerical examples are given to illustrate the approach.**

***Index Terms*—Continuation power flow, power flow, PV curve, three-phase power flow, voltage stability.**

I. Introduction

VOLTAGE stability has been recognized as a very important issue for operating power systems when the continuous load increase along with economic and environmental constraints has led to systems to operate close to their limits including voltage stability limit. In the past, various methodologies have been proposed for voltage stability analysis [1]–[4]. Among the voltage stability analysis methods, the continuation power-flow methods have been considered as one of the useful tools [5]–[11]. However, in the literature only application of the continuation power-flow methods in voltage stability analysis of positive-sequence power systems has been described.

Due to the following reasons: 1) there are unbalances of three-phase transmission lines in high voltage transmission networks; 2) there are unbalanced three phase loads; 3) in addition, there are one-phase or two-phase lines in distribution networks; 4) there are one-phase or two-phase loads; and 5) there may also be possible unbalanced three-phase structure and control of transformers and FACTS controllers, a CTPFlow may be required. In addition to the reasons above, with the recent integration of large amount of distributed generation into power networks, new voltage stability analysis tools, which should have the modeling capability of unbalanced networks, become increasingly important. Furthermore, it is recognized that voltage stability analysis should be able to deal with asymmetrical contingencies such as single-phase and two-phase transmission line outages, etc. It is known that the single-phase continuation power flow is not able to deal with unbalanced network and load, not mention to deal with single-phase and two-phase outages of unbalanced transmission lines.

In the light of the above considerations, in this paper, a CTPFlow approach for voltage stability analysis of unbalanced three-phase power systems is presented. The paper is arranged as follows. The modeling of synchronous machines and formulation of the three-phase power flow are described at first. Then CTPFlow approach is proposed. Numerical examples are given to show some unique characteristics of the PV curves of unbalanced three-phase power systems. Finally, general conclusions are drawn.

Manuscript received June 15, 2004; revised November 18, 2004. Paper no. TPWRS-00322–2004.

X.-P. Zhang is with the School of Engineering, University of Warwick, Coventry CV4 7AL, U.K. (e-mail: X.P.Zhang@warwick.ac.uk).

P. Ju is with the College of Electrical Engineering, HoHai University, Nanjing 210098, China (e-mail: pju@hhuc.edu.cn).

E. Handschin is with the Institute of Energy Systems and Energy Economics, Department of Electrical Engineering, University of Dortmund, 44221 Dortmund, Germany (e-mail: Edmund.Handschin@udo.edu).

Digital Object Identifier 10.1109/TPWRS.2005.851950

II. Three-Phase Power Flow in Polar Coordinates

A. Modeling of Synchronous Machines

A synchronous machine may be represented by a set of three-phase balanced voltage sources in series with a 3 by 3 impedance matrix. Such a synchronous machine model is shown in Fig. 1. The impedance matrix $\boldsymbol{Zg}_i$ may be determined by positive-, negative-, and zero-sequence impedance parameters of a synchronous machine. $\boldsymbol{Zg}_i$ is defined in Appendix A.

It is assumed the synchronous generator in Fig. 1 has a round rotor structure, and saturation of the synchronous generator is not considered in the present model. However, in principle, there is no difficulty to take into account the saturation.

In Fig. 1, $\boldsymbol{V}_i^a = V_i^a \angle \theta_i^a$, $\boldsymbol{V}_i^b = V_i^b \angle \theta_i^b$, $\boldsymbol{V}_i^c = V_i^c \angle \theta_i^c$, which are the three-phase voltages at the generator terminal bus, are expressed in phasors in polar coordinates. Similarly, the voltages at the generator internal bus may be given by $\boldsymbol{E}_i^a = E_i^a \angle \delta_i^a$, $\boldsymbol{E}_i^b = E_i^b \angle \delta_i^b$, $\boldsymbol{E}_i^c = E_i^c \angle \delta_i^c$. In fact the voltages at the generator internal bus are balanced, we have $E_i^a = E_i^b = E_i^c$ and $\delta_i^a = \delta_i^b + 120° = \delta_i^c - 120°$. Therefore, in the following derivation of the power-flow equations of the generator, δ_i^a and E_i^a can be considered as independent state variables of the internal generator bus while δ_i^b and E_i^b, δ_i^c and E_i^c are dependent state variables and can be represented by δ_i^a and E_i^a.

The total active and reactive powers at a generator terminal bus in polar coordinates can be represented as functions of the

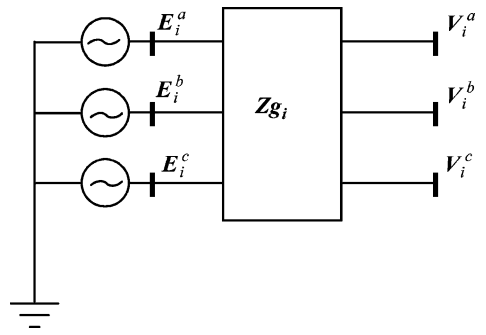

Fig. 1. Representation of a synchronous machine in three-phase power-flow analysis.

generator terminal and internal bus voltages and given by

$$\begin{aligned} Pg_i = &- \sum_{p=a,b,c} \sum_{m=a,b,c} V_i^p V_i^m \\ &\times \left(Gg_i^{pm} \cos\left(\theta_i^p - \theta_i^m\right) + Bg_i^{pm} \sin\left(\theta_i^p - \theta_i^m\right)\right) \\ &+ \sum_{p=a,b,c} \sum_{m=a,b,c} V_i^p E_i^m \\ &\times \left(Gg_i^{pm} \left(\theta_i^p - \delta_i^m\right) + Bg_i^{pm} \sin\left(\theta_i^p - \delta_i^m\right)\right) \end{aligned} \tag{1}$$

$$\begin{aligned} Qg_i = &- \sum_{p=a,b,c} \sum_{m=a,b,c} V_i^p V_i^m \left(Gg_i^{pm} \sin\left(\theta_i^p - \theta_i^m\right)\right. \\ &\left. - Bg_i^{pm} \cos\left(\theta_i^p - \theta_i^m\right)\right) \\ &+ \sum_{p=a,b,c} \sum_{m=a,b,c} V_i^p E_i^m \\ &\times \left(Gg_i^{pm} \sin\left(\theta_i^p - \delta_i^m\right) - Bg_i^{pm} \cos\left(\theta_i^p - \delta_i^m\right)\right) \end{aligned} \tag{2}$$

where $\boldsymbol{Gg}_i$ and $\boldsymbol{Bg}_i$, which are 3 by 3 matrix, are given by $\mathrm{Re}(\boldsymbol{Yg}_i)$ and $\mathrm{Im}(\boldsymbol{Yg}_i)$, respectively. $\boldsymbol{Yg}_i$ is defined by (31) in Appendix A, which is the inverse of $\boldsymbol{Zg}_i$. Pg_i and Qg_i, which are the total active and reactive power at the generator terminal bus, have the direction of leaving the internal bus and toward the terminal bus. As mentioned above, in (1) and (2) actually δ_i^b and δ_i^c, E_i^b and E_i^c can be represented by δ_i^a and E_i^a, respectively.

Similar to that in the single-phase power-flow analysis, synchronous machine terminal buses can be classified as Slack Bus, PV Buses, and PQ Buses, respectively. Accordingly, the synchronous machines may be classified as Slack machine, PV machines and PQ machines. The power and voltage constraint equations for Slack Bus, PV Buses, and PQ Buses of synchronous machines are presented as follows.

1) Slack Machine: At the terminal bus of the Slack machine, the positive-sequence voltage magnitude is specified and the positive-sequence voltage angle is taken as the system reference. We have

$$\Delta\theta g_i = f_i^1 = 0 \tag{3}$$

$$\Delta V g_i = V_i^{Spec} - \sqrt{\left(e_i^1\right)^2 + \left(f_i^1\right)^2} = 0 \tag{4}$$

where V_i^{Spec} is the specified positive-sequence voltage at the terminal bus of the slack machine. e_i^1 and f_i^1 are the real and imaginary parts of the positive-sequence voltage at the terminal bus of the Slack machine and given by

$$e_i^1 = \frac{\mathrm{Re}\left(\boldsymbol{V}_i^a + \boldsymbol{V}_i^b e^{j120^\circ} + \boldsymbol{V}_i^c e^{j240^\circ}\right)}{3} \tag{5}$$

$$f_i^1 = \frac{\mathrm{Im}\left(\boldsymbol{V}_i^a + \boldsymbol{V}_i^b e^{j120^\circ} + \boldsymbol{V}_i^c e^{j240^\circ}\right)}{3} \tag{6}$$

where $\boldsymbol{V}_i^a$, $\boldsymbol{V}_i^b$ and $\boldsymbol{V}_i^c$ are the phase a, phase b and phase c voltages at bus i, respectively.

2) PV Machines: At the terminal bus of a PV machine, the total active power and the positive-sequence voltage magnitude are specified. We have

$$\Delta Pg_i = Pg_i^{Spec} - Pg_i = 0 \tag{7}$$

$$\Delta V g_i = V_i^{Spec} - \sqrt{\left(e_i^1\right)^2 + \left(f_i^1\right)^2} = 0 \tag{8}$$

where P_i^{Spec} and V_i^{Spec} are the specified total active power and the positive-sequence voltage at the terminal bus of the PV machine. Pg_i is the total actual active power at the terminal bus and given by (1). e_i^1 and f_i^1 are the real and imaginary parts of the positive-sequence voltage, respectively, which are given by (5) and (6), respectively.

For a PV machine, the total reactive power Qg_i at its terminal bus should be within its operating limits

$$Qg_i^{min} \le Qg_i \le Qg_i^{max} \tag{9}$$

where Qg_i^{min} and Qg_i^{max} are the lower and upper reactive limits, respectively. In addition, due to the limitation of the field current, the following constraint should hold:

$$E_i^a \le E_i^{max} \tag{10}$$

where E_i^{max} is the maximum limit of the internal voltage of the machine, which corresponds to the maximum filed current. E_i^a is the actual voltage magnitude at the internal bus.

3) PQ Machines: At the terminal bus of a PQ machine, the total active and reactive powers are specified. We have

$$\Delta Pg_i = Pg_i^{Spec} - Pg_i = 0 \tag{11}$$

$$\Delta Qg_i = Qg_i^{Spec} - Qg_i = 0 \tag{12}$$

where P_i^{Spec} and Q_i^{Spec} are the specified total active and reactive powers at the terminal bus of the PQ machine. Pg_i and Qg_i are the total actual active and reactive powers, which are given by (1) and (2), respectively.

For a PQ machine, the positive-sequence voltage V_i^1 at its terminal bus should be within its operating limits

$$V_i^{min} \le V_i^1 \le V_i^{max} \tag{13}$$

where V_i^{min} and V_i^{max} are the upper and lower voltage limits, respectively. In addition, the field current constraint as given by (10) is also applicable.

The basic constraint enforcement principle of a synchronous machine is that, when there is an inequality constraint such as the current or voltage or reactive power inequality constraint is violated, the constraint is enforced by being kept at its limit, while the voltage or reactive power control constraint of the synchronous machine is released. In other words, enforcing an inequality constraint and releasing an equality constraint must form a pair. In case there are two or more inequality constraints of a synchronous machine being violated in the same time, the strategy proposed in [21] can be used. The reactive power constraint in (9) and current constraint in (10) of a machine are considered as internal constraints while the voltage constraint in (13) is considered as an external constraint. Generally, an internal constraint has priority to be enforced if both the internal and external constraints are violated simultaneously. In case the internal and external constraints cannot be enforced within the limits simultaneously, the external constraint should be released.

Modeling of other power system components such as transmission lines, transformers, etc. in three-phase power-flow analysis can be found in [12].

B. Three-Phase Power Flow

The power-flow equations at buses except generator internal buses in polar coordinates may be given by

$$P_i^p = \sum_{j\in i,m=a,b,c} V_i^p V_j^m \times \left(G_{ij}^{pm}\cos\left(\theta_i^p-\theta_j^m\right)+B_{ij}^{pm}\sin\left(\theta_i^p-\theta_j^m\right)\right) \quad (14)$$

$$Q_i^p = \sum_{j\in i,m=a.b.c} V_i^p V_j^m \times \left(G_{ij}^{pm}\sin\left(\theta_i^p-\theta_j^m\right)-B_{ij}^{pm}\cos\left(\theta_i^p-\theta_j^m\right)\right) \quad (15)$$

where the subscript i and j represent the bus number while the superscript p and m represent the phase.

The power mismatch equations at buses except generator internal buses may be given by

$$\Delta P_i^p = -Pd_i^p - P_i^p = 0 \quad (16)$$

$$\Delta Q_i^p = -Qd_i^p - Q_i^p = 0 \quad (17)$$

where Pd_i^p and Qd_i^p are the active and reactive load powers of phase p at bus i, respectively. P_i^p and Q_i^p, which are given by (14) and (15), are the sum of the active and reactive power flows of phase p at bus i, respectively.

A number of three-phase power-flow methods [13]–[20], etc. have been proposed since 1960s. In the following, the three-phase Newton power-flow algorithm in polar coordinates, which is similar to that proposed in [15], will be described. The nonlinear equations (3), (4), (7), (8), (11), (12), (16) and (17) can be combined and expressed in compact form

$$\boldsymbol{f}(\boldsymbol{x}) = \mathbf{0} \quad (18)$$

where $\boldsymbol{f}(\boldsymbol{x})$ represents the whole set of power-flow mismatch and machine terminal constraint equations. $\boldsymbol{x}$ is the state variable vector and given by $\boldsymbol{x} = [\boldsymbol{\theta}^{\mathbf{a}}, \mathbf{V}^{\mathbf{a}}, \boldsymbol{\theta}^{\mathbf{b}}, \mathbf{V}^{\mathbf{b}}, \boldsymbol{\theta}^{\mathbf{c}}, \mathbf{V}^{\mathbf{c}}, \boldsymbol{\delta}^{\mathbf{a}}, \mathbf{E}^{\mathbf{a}}]^t$.

The Newton equation is given by

$$\boldsymbol{J}(\boldsymbol{x})\Delta\boldsymbol{x} = -\boldsymbol{f}(\boldsymbol{x}) \quad (19)$$

where $\boldsymbol{J}(\boldsymbol{x}) = \partial\boldsymbol{f}(\boldsymbol{x})/\partial\boldsymbol{x}$ is the system Jacobian matrix.

III. Continuation Three-Phase Power Flow

A. Predictor Step

To simulate load change, Pd_i^p and Qd_i^p, which are shown in (16) and (17), may be represented by

$$Pd_i^p = Pd0_i^p\left(1+\lambda^* KPd_i^p\right) \quad (20)$$

$$Qd_i^p = Qd0_i^p\left(1+\lambda^* KQd_i^p\right) \quad (21)$$

where $Pd0_i^p$ and $Qd0_i^p$ are the base case active and reactive load powers of phase p at bus i. λ is the loading factor, which characterize the change of load. The ratio of KPd_i^p/KQd_i^p is constant to maintain constant power factor.

Similarly, to simulate generation change, Pg_i and Qg_i, which are shown in (7), (11) and (12), are represented as functions of λ and are given by

$$Pg_i = Pg0_i\left(1+\lambda^* KPg_i\right) \quad (22)$$

$$Qg_i = Qg0_i\left(1+\lambda^* KQg_i\right) \quad (23)$$

where $Pg0_i$ and $Qg0_i$ are the total active and reactive powers of the generator of the base case. The ratio of KPg_i/KQg_i is constant to maintain constant power factor for a PQ machine. For a PV machine, (23) is not required. For a machine, when the reactive limit is violated, Qg_i should be kept at the limit and (23) is also not required.

The nonlinear equations (18) are augmented by an extra variable λ as follows:

$$\mathbf{f}(\mathbf{x},\lambda) = \mathbf{0} \quad (24)$$

where $\boldsymbol{f}(\boldsymbol{x},\lambda)$ represents the whole set of power-flow mismatch equations.

The predictor step is used to provide an approximate point of the next solution. A prediction of the next solution is made by taking an appropriately sized step in the direction tangent to the solution path.

To solve (24), the continuation algorithm with predictor and corrector steps can be used. Linearizing (24), we have

$$d\boldsymbol{f}(\boldsymbol{x},\lambda) = \boldsymbol{f}_x d\boldsymbol{x} + \boldsymbol{f}_\lambda d\lambda = 0. \quad (25)$$

In order to solve (25), one more equation is needed. If we choose a nonzero magnitude for one of the tangent vector and keep its change as ± 1, one extra equation can be obtained

$$t_k = \pm 1 \quad (26)$$

where t_k is a nonzero element of the tangent vector $d\boldsymbol{x}$.

Combining (25) and (26), we can get a set of equations where the tangent vector $d\boldsymbol{x}$ and $d\lambda$ are unknown variables.

$$\left[\begin{array}{c|c}\boldsymbol{f}_x & \boldsymbol{f}_\lambda \\ \hline e_k\end{array}\right]\left[\begin{array}{c} d\boldsymbol{x} \\ \hline d\lambda\end{array}\right] = \left[\begin{array}{c}\mathbf{0} \\ \hline \pm\mathbf{1}\end{array}\right] \quad (27)$$

where e_k is a row vector with all elements zero except for K^{th}, which equals one. In (27), whether $+1$ or -1 is used depends on how the K^{th} state variable is changing as the solution is being traced. After solving (27), the prediction of the next solution may be given by

$$\begin{bmatrix} \mathbf{x}^* \\ \hline \lambda^* \end{bmatrix} = \begin{bmatrix} \mathbf{x} \\ \hline \lambda \end{bmatrix} + \sigma \begin{bmatrix} d\mathbf{x} \\ \hline d\lambda \end{bmatrix} \tag{28}$$

where $*$ denotes the estimated solution of the next step while σ is a scalar, which represents the step size.

B. Corrector Step

The corrector step is to solve the augmented Newton power-flow equation with the predicted solution in (28) as the initial point. In the augmented Newton power-flow algorithm an extra equation is included and λ is taken as a variable. The augmented Newton power-flow equation may be given by

$$\begin{bmatrix} \boldsymbol{f}(\boldsymbol{x}, \lambda) \\ \hline x_k - \eta \end{bmatrix} = \begin{bmatrix} \mathbf{0} \\ \hline 0 \end{bmatrix} \tag{29}$$

where η, which is determined by (28), is the predicted value of the continuation parameter x_k. The determination of the continuation parameter is shown in the following solution procedure.

The corrector (29), which consists a set of augmented nonlinear equations, can be solved iteratively by Newton's approach as follows:

$$\begin{bmatrix} \boldsymbol{f}_x & \boldsymbol{f}_\lambda \\ \hline e_k & \end{bmatrix} \begin{bmatrix} \Delta \boldsymbol{x} \\ \hline \Delta \lambda \end{bmatrix} = - \begin{bmatrix} \boldsymbol{f}(\boldsymbol{x}, \lambda) \\ \hline x_k - \eta \end{bmatrix}. \tag{30}$$

C. Solution Procedure

The general solution procedure for the CTPFlow is given as follows.

Step 0: Run three-phase power flow when Pd_i^p, Qd_i^p, Pg_i and Qg_i are set to $Pd0_i^p$, $Qd0_i^p$, $Pg0_i$ and $Qg0_i$, respectively. The initial point for tracing the PV curves is found.

Step 1: Predictor Step:

(a) Solve (27) and get the tangent vector $[d\boldsymbol{x}, d\lambda]^t$

(b) Use (28) to find the predicted solution of the next step.

(c) Choose the continuation parameter by evaluating x_k : $t_k = \max(|dx_i|)$.

(d) Check whether the critical point (maximum loading point) has been passed by evaluating the sign of $d\lambda$. If $d\lambda$ changes its sign from positive to negative, then the critical point has just passed.

(e) Check whether $\lambda^* < 0$ (Note $0 \le \lambda \le \lambda_{\max}$). If this is true, go to Step 3.

Step 2) Corrector Step:

(a) According to the chosen continuation parameter to form the augmented (29);

(b) Form and solve the Newton equation (30);

(c) Update the Newton solution and continue the iterations until the corrector step converges to a solution with a given tolerance;

(d) Go to Step 1.

Step 3) Output solutions of the PV curves.

D. Implementation Issues

1) The Structure of Jacobian Matrix: The structures of the Jacobian matrix (27) and the Jacobian matrix (30) are very similar. In comparison to the 4 by 4 Jacobian blocks in single-phase power-flow analysis, the Jacobian matrix blocks of $\boldsymbol{f}_x$ in three-phase power-flow analysis become 12 by 12 matrix blocks for all buses except internal buses of generators while the Jacobian blocks of the internal buses of generators are 4 by 4, 4 by 12, 12 by 4 matrix blocks. Similar to that of single-phase power-flow analysis, the (27) and (30) of three-phase power systems can be solved by sparse matrix techniques.

2) Improvement of Computational Speed: In order to improve the computational speed for tracing the PV curves, in the implementation, the three-phase power-flow calculations may be used with gradually increasing system load until the three-phase power flow cannot converge. Then the above CTPFlow approach can be used to trace the remaining parts of the PV curves. Using the three-phase continuation power flow, a small predictor step may be used at the vicinity of the point of voltage collapse while a large step may be used otherwise.

In the present implementation of the CTPFlow algorithm, the tangent method is used at the predictor step. It has been recognized that the tangent method may be more reliable than the secant method. In addition, the tangent method can produce an approximate left eigenvector at the saddle node bifurcation point. However, as far as computational time is concerned, the secant method may be more attractive [10] since using the method, solution of (27) is not needed.

On the other hand, the solution of (27) may be significantly improved by using the sparse vector method [22] in the future implementation. Since the only one nonzero element of the right-hand vector in (27) is at the bottom, the forward substitution is not needed at all.

3) Comparison of the Singularity Between Balanced Three-Phase Systems and Single-Phase Systems: It should be pointed out that for a balanced system, a three-phase power-flow solution is, in principle, exactly identical to that of the equivalent positive-sequence power flow while positive-and zero-sequence voltage components of the former are zero and at any bus, phase a, b and c voltages are balanced and interdependent except 120° shifting between them. In other words, for a balanced three-phase power system, any phase voltage at a bus can completely characterize the positive-sequence voltage at that bus. Mathematically, the balanced three-phase system can be decoupled into the equivalent positive-, negative-, and zero-sequence networks, and the singularity resulting from the equivalent positive-sequence network can be solved by choosing any phase voltage at the bus as the continuation parameter. This means, in nature, the reason and solution of the singularity of the balanced three-phase power flow are exactly the same to that of the equivalent positive-sequence power flow. The difference between them is whether the system is represented in three-phase or single-phase coordinates.

4) Modeling of Advanced Power System Control Components: In principle, similar to the single-phase analysis, there are no inner limitations for modeling of FACTS controllers, excitation systems, and tap changers in three-phase system

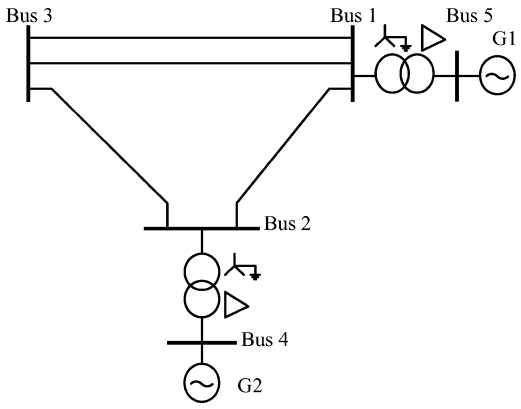

Fig. 2. 5-bus three-phase power network.

analysis. It can be anticipated that explicitly modeling of excitation systems, tap changer control would be more likely to reflect the regulating characteristics of power system components and improve the accuracy of the computational results. It can also be anticipated that modeling of FACTS in three-phase analysis is much more complicated than that in single-phase analysis. Clearly further research in these aspects of three-phase modeling and analysis is expected.

IV. Numerical Results

A. Test Systems

In this paper, numerical results are carried out on a 5-bus system and a modified IEEE 118-bus system. The 5-bus system single-line diagram is shown in Fig. 2 while the system data are presented in Appendix B. For the modified IEEE 118-bus system, 54 three-phase Wye-Grounded/Delta transformers are inserted between the original network and 54 generators and negative- and zero-sequence parameters of transmission lines are amended. The modified IEEE 118-bus system consists of 172 three-phase buses (or 516 single-phase buses). In the studies, loads are represented by P and Q powers.

B. Case Studies on the 5-Bus System

1) Cases on the 5-Bus System Without Line Outages: The following cases on the 5-bus network have been studied:

- Case 1: balanced network and the whole system with balanced load.
- Case 2: balanced network with unbalanced load at Bus 3 with $6.0 + j3.0$ p.u., $6.3 + j2.7$ p.u., $5.7 + j3.3$ p.u. for phase a, b, c loading, respectively.
- Case 3: unbalanced network and the whole system with balanced load.
- Case 4: unbalanced network with unbalanced load at Bus 3 with $6.0 + j3.0$ p.u., $6.3 + j2.7$ p.u., $5.7 + j3.3$ p.u. for phase a, b, c loading, respectively.

The PV curves of Cases 1–4 are shown in Figs. 3–6. It is known that the tracing direction of the PV curves of a single-phase or positive-sequence system is clockwise. From Fig. 3, it can be seen that for the balanced three-phase power system, the three PV curves at any bus are exactly the same and the tracing direction of these PV curves is clockwise.

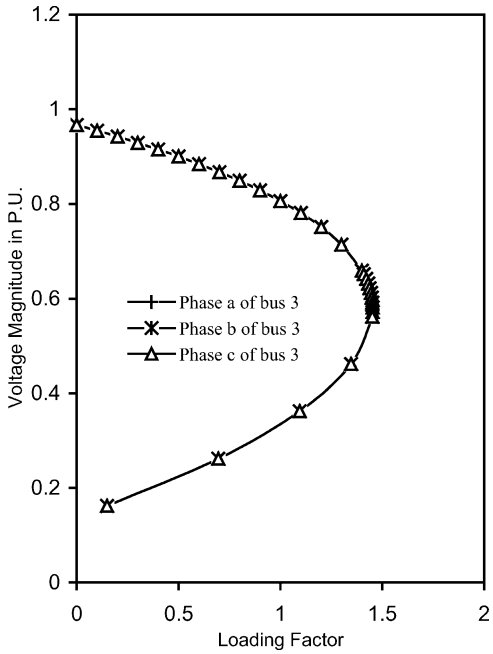

Fig. 3. PV curves of bus 3 for Case 1.

As expected, the three PV curves for phase a, phase b and Phase c at Bus 3 of Case 1 are exactly the same. Furthermore, these PV curves have very similar pattern to that of a single-phase or positive-sequence power system. That is each PV curve consists of a high voltage portion and a low voltage portion. As the loading factor λ is increasing between 0 and $\lambda_{\max}$, the operating point of the system is moving from the initial point to the maximum loading point or the point of voltage collapse, which is corresponding to the higher voltage portion of the PV curve. After the point of voltage collapse, the loading factor λ is decreasing from $\lambda_{\max}$ to 0, which is corresponding to the lower voltage portion of the PV curve. It is known that any points on the lower voltage portion are unstable.

Having discussed the PV curves for single-phase and examined also the PV curves of balanced three-phase systems, the PV curves of unbalanced three-phase systems are to be discussed here. It has been found that the three PV curves for phase a, phase b and Phase c at Bus 3 for any of Case 2–4, are not the same. Examining the PV curves at Bus 3 of Case 2 shown in Fig. 4, it was interestingly found.

1) In the PV curves of Phases a and c, the voltages are decreasing when λ is increasing between 0 and $\lambda_{\max}$. The tracing direction of these two PV curves is clockwise and the patterns of these two PV curves are very similar to that of single-phase or balanced three phase power systems.
2) However, in the PV curve of phase b, the voltage is decreasing till at a point close to the point of $\lambda_{\max}$, then the voltages become increasing. The tracing direction of the PV curve is anti-clockwise. In this PV curve, the "higher voltage" portion is corresponding to the unstable power-flow solutions while the "lower voltage" portion is corresponding to the stable power-flow solutions.

Further examining the PV curves of Case 3 and 4 shown in Figs. 5 and 6, respectively, it can be found.

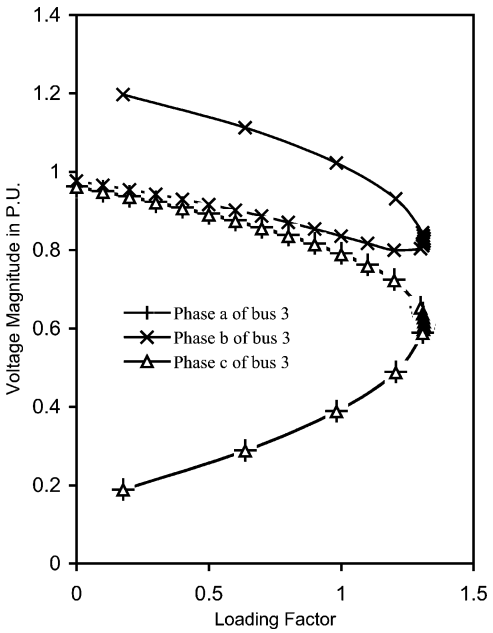

Fig. 4. PV curves of bus 3 for Case 2.

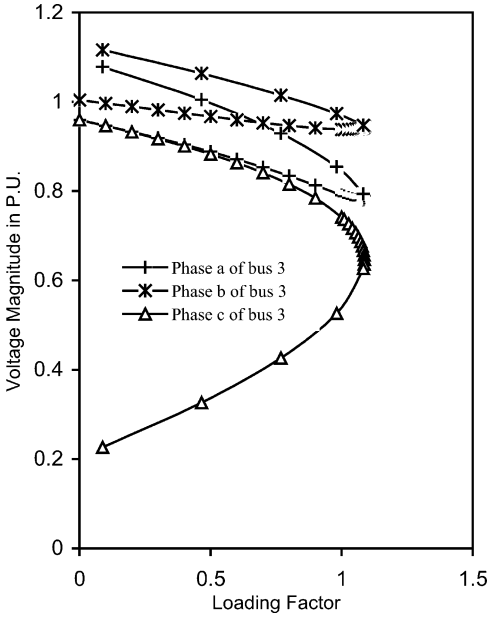

Fig. 5. PV curves of bus 3 for Case 3.

1) The patterns of the PV curves of the unbalanced three-phase systems are quite different from that of the balanced three-phase systems. At least one of the PV curves at a bus has the clockwise tracing direction and the voltage of the phase is much lower than that of the other phases while the PV curves of the other phases may have the anti-clockwise tracing direction.
2) However, when the network and load are balanced, the three PV curves at any bus merge into one as seen in Fig. 3. Then a positive-network analysis is sufficient.
3) Voltage stability analysis of unbalanced three-phase power systems are much more complex than that of single-phase positive sequence power systems or balanced three-phase power systems.

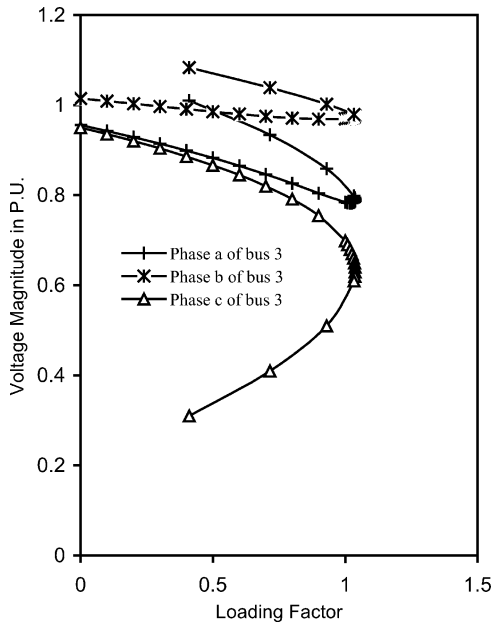

Fig. 6. PV curves of bus 3 for Case 4.

TABLE I
MAXIMUM LOADING FACTORS WITHOUT LINE OUTAGES

Case no	Maximum loading factor λ_{max}	Lowest voltage magnitude (in p.u.) at maximum loading point	Bus no of the lowest voltage	Phase of the lowest voltage
1	1.45296	0.5818	3	*a, b, c*
2	1.31274	0.6095	3	*a*
3	1.08638	0.6465	3	*c*
4	1.03741	0.6299	3	*c*

The maximum loading factors for Cases 1–4 are shown in Table I. From Table I, it can be clearly seen that unbalanced network and load can significantly affect the system loading capability.

2) Cases on the 5-Bus System With Line Outages: In order to investigate the voltage stability of unbalanced three-phase systems where there are transmission line outages, the following Cases were carried out.

Case 5: This is similar to Case 4 but Phase a of one of the double lines between Bus 1 and Bus 3 is open-circuited.

Case 6: This is similar to Case 4 but Phase b of one of the double lines between Bus 1 and Bus 3 are open-circuited.

Case 7: This is similar to Case 4 but the Phase c of one of the double lines between Bus 1 and Bus 3 are open-circuited.

Case 8: This is similar to Case 4 but Phase a and Phase b of one of the double lines between Bus 1 and Bus 3 is open-circuited.

Case 9: This is similar to Case 4 but Phase b and Phase c of one of the double lines between Bus 1 and Bus 3 are open-circuited.

TABLE II
MAXIMUM LOADING FACTORS WITH LINE OUTAGES

Case no	Type of line outage	Maximum loading factor λ_{max}	Lowest voltage magnitude (in p.u.) at maximum loading point	Bus no of the lowest voltage	Phase of the lowest voltage
5	Phase *a*	0.68780	0.6183	3	*a*
6	Phase *b*	1.06272	0.6329	3	*c*
7	Phase *c*	0.53173	0.6182	3	*c*
8	Phases *a* and *b*	0.56810	0.6067	3	*a*
9	Phases *b* and *c*	0.59865	0.6329	3	*c*
10	Phases *a* and *c*	0.51763	0.6147	3	*c*
11	Phases *a*, *b* and *c*	0.56649	0.6407	3	*c*

Case 10: This is similar to Case 4 but Phase c and Phase a of one of the double lines between Bus 1 and Bus 3 are open-circuited.

Case 11: This is similar to Case 4 but Phase a, Phase b and Phase c of one of the double lines between Bus 1 and Bus 3 are open-circuited.

The maximum loading factors for Cases 5–11 are shown in Table II. From Table II, the following can be seen.

1) Surprisingly, the maximum loading factor of Case 6 (with line 1–3 outage on phase b) is greater than that of Case 4 without any line outage. This means that for the unbalanced three-phase system studied, Case 6 with single-phase line outage is less serious than Case 4 without line outages in the point of view of voltage stability.
2) Among the single-phase line outages of Cases 5–7, Case 6 is less serious than the other two Cases. The maximum loading factor of Case 6 is about two times that of the other two Cases, respectively.
3) Cases 8 and 9 with two-phase line outages have larger loading factors than Case 7 with one-phase line outage. This means that for the unbalanced three-phase system studied, the two-phase line outages of Cases 8 and 9 are less serious than the one-phase line outage of Case 7 in the point of view of voltage stability.
4) Case 11 with three-phase line outage has larger loading factor than Case 7 with one-phase line outage and Case 10 with two-phase line outages. This means that the three-phase line outage of Case 11 is less serious than the one-phase line outage of Case 7 and the two-phase line outage of Case 10 in the point of view of voltage stability.

The above observations are very interesting phenomena from the unbalanced three-phase systems, which are quite different from that of single-phase systems or balanced three-phase systems. Due to the combinations of the complexity of unbalanced load and network, it is not easy to explain qualitatively the above observations. Instead, we try to show numerical results to reveal the possible reasons for the above phenomena. The three-phase power-flow results of Cases 4–11 at particular loading levels are shown in Table III and Table IV respectively. In the tables, V_3^1, V_3^2 and V_3^0 are the positive-, negative-, zero-sequence voltage magnitudes at bus 3, respectively while voltage sensitivities, which are the largest in magnitude for the corresponding Cases, are shown in the last column of these two Tables.

TABLE III
POWER FLOW RESULTS AT $\lambda = 0.5$ (VOLTAGE AND POWER IN p.u.)

Case no	V_3^1	V_3^2	V_3^0	P_{loss}	Q_{loss}	Normalized Q_{loss}	$\frac{\partial V}{\partial \lambda}$
4	0.9117	**0.0378**	**0.0403**	1.33	8.89	**100%**	**-0.21**
5	0.8837	**0.0567**	**0.0857**	1.62	11.09	**125%**	**-0.41**
6	0.8983	**0.0276**	**0.0154**	1.45	10.00	**113%**	**-0.20**
7	0.8602	**0.1037**	**0.1133**	1.76	12.77	**144%**	**-1.14**
8	0.8672	**0.0636**	**0.1193**	1.85	13.04	**147%**	**-0.74**
9	0.8621	**0.0727**	**0.0599**	1.74	12.51	**141%**	**-0.59**
10	0.8373	**0.0910**	**0.1312**	2.02	14.74	**166%**	**-1.51**
11	0.8452	**0.0788**	**0.0946**	1.99	14.22	**160%**	**-0.70**

TABLE IV
POWER FLOW RESULTS AT $\lambda = 1.03$ (VOLTAGE AND POWER IN p.u.)

Case no	V_3^1	V_3^2	V_3^0	Lowest phase voltage	P_{loss}	Q_{loss}	$\frac{\partial V}{\partial \lambda}$
4	0.8042	**0.0887**	**0.1087**	**0.6629**	3.18	24.70	-1.94
6	0.7966	**0.0540**	**0.0333**	**0.6971**	3.38	26.39	-0.88

The voltage sensitivities can be considered as an indicator of voltage instability. In principle, the larger the voltage sensitivity is, the lower the maximum loading factor will be. The voltage sensitivities in Table III and Table IV correlate well with the maximum loading factors of Case 4–11. In addition, it has been found that for most of the Cases, high power losses and negative- and zero-sequence voltage components are associated with large voltage sensitivities.

Comparing the results of Case 4 and Case 6 in Table III and Table IV, the following can be seen.

1) At $\lambda = 0.5$, the largest voltage sensitivity of Case 4 is larger than that of Case 6.
2) As λ is increased to 1.03, the voltage sensitivity of Case 4 becomes much larger than that of Case 6. The voltage sensitivities indicate that Case 4 is more vulnerable to voltage instability and hence a lower maximum loading factor is expected for this Case.

3) Reactive Power Limits: For Case 4, with generator reactive power limits applied, the PV curves of bus 3 are shown in Fig. 7.

From Fig. 7, the following can be found.

1) In comparison of Fig. 7 to Fig. 6, as expected, the maximum loading factor is decreased when the generator reactive power limits are applied.
2) The significant reduction in the voltage magnitudes of phases a and b can be seen when the generator reactive power limits are encountered. Phase c voltage magnitudes are actually reduced as well.
3) The effect of the reactive power limits is the reduction in bus voltage magnitudes. In other words, the three PV curves move down since the generator terminal bus

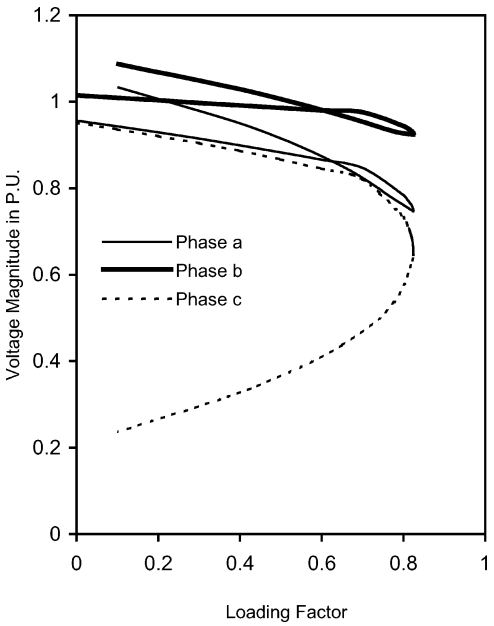

Fig. 7. PV curves of bus 3 for Case 4 with generator reactive power limits.

voltage cannot hold up to the setting point any longer. Noting the tracing direction of the PV curves of phases a and b is anti-clockwise, the effect of the reactive power limits on the voltage magnitudes of these two phases is more significant and delays the voltage rise of phases a and b. Hence, the effect causes the "higher portion" of the PV curves fall and cross the "lower portion" of these.

C. Case Studies on the Modified IEEE 118-Bus System

The following four Cases were carried out on the modified IEEE 118-bus system with balanced network and load:

Case 12: This is the Base Case system.

Case 13: This is similar to Case 12 but one phase of the line between Bus 68 and Bus 81 is open-circuited.

Case 14: This is similar to Case 12 but two phases of the line between Bus 68 and Bus 81 are open-circuited.

Case 15: This is similar to Case 12 but three phases of the line between Bus 68 and Bus 81 are open-circuited.

The maximum loading factors for Cases 12–15 on the modified IEEE 118-bus system are shown in Table V.

TABLE V
MAXIMUM LOADING FACTORS ON THE MODIFIED IEEE 118-BUS SYSTEM

Case no	Maximum loading factor λ_{max}	Type of line outage
12	0.6910	None
13	0.6599	One phase outage of line 68-81
14	0.5998	Two phase outage of line 68-81
15	0.5010	Three-phase outage of line 68-81

V. CONCLUSION

In this paper, a CTPFlow approach for voltage stability analysis of unbalanced three-phase power systems has been proposed. The approach can take into account the unbalances of both network and load. In addition, it can also deal with various transmission line outages.

Numerical examples have demonstrated the approach proposed is effective. Some very interesting results using PQ loads have been obtained:

1) When network and load are balanced, the PV curves of phase a, phase b and phase c at a bus are identical as expected and the pattern of these is very similar to that of the PV curves of single-phase power systems. In this situation, a single-phase positive network analysis is sufficient.
2) However, when network and load are unbalanced, the patterns of the PV curves are very interesting, which have not been observed and discussed yet in open references. It has been found that with unbalanced network and load, at least one of the PV curves at a bus is very similar to that of single-phase or balanced three-phase systems and the tracing direction of the PV curve is clockwise while the rest of the PV curves (or curve) at the bus have the anti-clockwise tracing direction. For those PV curves with anti-clockwise tracing direction, the higher voltage portion of the PV curves is corresponding to the unstable power-flow solutions while the lower voltage portion of the PV curves is corresponding to the stable power-flow solutions. The characteristic is unique to unbalanced three-phase power systems.
3) It has been found for unbalanced power systems that: a) the maximum loading factor of the system with a single-phase line outage may be greater than that of the system without any line outages; b) the maximum loading factor of the system with a two-phase line outage may not be necessarily less than that of the system with a single-phase line outage; and c) similarly, the maximum loading factor of the system with a three-phase line outage may not be necessarily less than that of the system with a single-phase line outage or a two-phase line outage. The phenomena have been explained based on numerical analyses. Basically, the maximum loading factor is dependent on the degree of unbalance, which is characterized by the magnitudes of negative- and zero-sequence voltages. The degree of unbalance itself is determined by the combination of unbalanced network and loading conditions.

The phenomena observed above reveal that the voltage stability mechanisms of three phase power systems are much more complex than that of single-phase power systems. This clearly indicates that a CTPFlow is needed when there are unbalanced network and load existing in a power system. Otherwise, the results may be unrealistic and could not be able to characterize accurately the voltage stability problem of unbalanced power systems.

Similar to that in conventional continuation power-flow analysis, reactive power limits of generators play a very important role in the determination of PV curves of three-phase power systems. Basically consideration of the reactive power limits will decrease the maximum loading factor and affect the shape of the PV curves. When the reactive power limits are taken into

account, there is the reduction in voltage magnitudes, and subsequently this will affect the shape of the PV curves. It has been found that the effect of the reactive power limits on the PV curves whose tracing direction is anti-clockwise is more significant than on those whose tracing direction is clockwise.

The present results are based on the PQ load model. Further research is needed to investigate the effect of voltage dependent load models on the voltage stability of unbalanced three phase power systems.

The CTPFlow approach will be a very useful tool for voltage stability of unbalanced three-phase power systems. The approach can also be used to investigate multiple power-flow solutions of unbalanced three-phase power systems.

As distributed generators are increasingly connected to power systems, the CTPFlow approach may become an important tool to evaluate the unbalanced system operation conditions including contingencies.

APPENDIX A
THE DEFINITION OF $\boldsymbol{Yg}_i$

$\boldsymbol{Zg}_i$ is the impedance matrix of a synchronous machine, which is given by (31), shown at the bottom of the page. where T_{abc}^{120} and T_{120}^{abc} are the transformation matrix of symmetrical components and its inverse matrix, respectively. z_1, z_2 and z_0 are the positive-, negative-, and zero-sequence impedances of a synchronous machine. $a = e^{j(2\pi/3)}$.

$\boldsymbol{Yg}_i$ is the admittance matrix of a synchronous machine, which is given by

$$\boldsymbol{Yg_i} = (\boldsymbol{Zg_i})^{-1} \tag{32}$$

APPENDIX B
5-BUS SYSTEM DATA

TABLE VI
GENERATOR DATA IN p.u.

Generator name	Bus no	Sequence impedances			Power	Voltage
		z_1	z_2	z_0	P_i^{Spec}	V_i^{Spec}
G1	5	0.0+*j*0.20	0.0+*J*0.04	0.0+*J*0.02	21.0	1.061
G2	4	0.0+*j*0.20	0.0+*J*0.04	0.0+*J*0.02	Slack	1.045

TABLE VII
TRANSFORMER DATA IN p.u.

Transformer	T1 & T2
Connection	Wye-G/Delta
Leakage impedance	0.0016+*j*0.015
Primary tap	1.0
Secondary tap	1.0

TABLE VIII
UNBALANCED LINE DATA FOR LINE 1–2, LINE 1–3 AND LINE 2–3

Series impedance matrix (p.u.)		
Phase a	*Phase b*	*Phase c*
0.0066 + *j* 0.0560	0.0017 + *j* 0.0270	0.0012 + *j* 0.0210
	0.0045 + *j* 0.0470	0.0014 + *j* 0.0220
		0.0062 + *j* 0.0610
Shunt admittance matrix (p.u.)		
Phase a	*Phase b*	*Phase c*
j 0.150	- *j* 0.030	- *j* 0.010
	j 0.250	- *j* 0.020
		j 0.125

TABLE IX
LOAD DATA OF THE 5-BUS SYSTEM

	Phase *a*	Phase *b*	Phase *c*
Bus 1	0.6 + j 0.3	0.6 + j 0.3	0.6 + j 0.3
Bus 2	2.0 + j 0.8	2.0 + j 0.8	2.0 + j 0.8
Bus 3	6.0 + j 3.0	6.0 + j 3.0	6.0 + j 3.0

REFERENCES

[1] Y. Mansour, Ed., *Suggested Techniques for Voltage Stability Analysis*: IEEE Power Engineering Society, 1993.

[2] P. Kundur, *Power System Stability and Control*. New York: McGraw-Hill, 1994.

[3] C. W. Taylor, *Power System Voltage Stability*. New York: McGraw-Hill, 1994.

[4] T. Van Cutsem and C. Vournas, *Voltage Stability of Electric Power Systems*. Norwell, MA: Kluwer, 1998.

[5] M. Huneault, A. Fahmideh-Vodani, M. Juman, and F. G. Galiana, "The continuation method in power system optimization: applications to economy security functions," *IEEE Trans. Power App. Syst.*, vol. PAS-104, no. 1, pp. 114–124, 1985.

[6] M. Huneault and F. G. Galiana, "An investigation of the solution to the optimal power flow problem incorporating continuation methods," *IEEE Trans. Power Syst.*, vol. 5, no. 1, pp. 103–110, Feb. 1990.

[7] K. Iba, H. Suzuki, M. Egawa, and T. Watanabe, "Calculation of critical loading condition with nose curve using homotopy continuation method," *IEEE Trans. Power Syst.*, vol. 5, no. 1, pp. 103–110, Feb. 1990.

[8] V. Ajjarapu and C. Christy, "The continuation power flow: a tool for steady state voltage stability analysis," *IEEE Trans. Power Syst.*, vol. 7, no. 1, pp. 416–423, Feb. 1992.

[9] C. A. Canizares and F. L. Alvarado, "Point of collapse and continuation methods for large ac/dc systems," *IEEE Trans. Power Syst.*, vol. 8, no. 1, pp. 1–8, Feb. 1993.

[10] H.-D. Chiang, K. S. Shah, and N. Balu, "CPFLOW: A practical tool for tracing power system steady-state stationary behavior due to load and generation variations," *IEEE Trans. Power Syst.*, vol. 10, no. 2, pp. 623–634, May 1995.

[11] G. C. Ejebe, J. Tong, J. G. Waight, J. G. Frame, X. Wang, and W. F. Tinny, "Available transfer capability calculations," *IEEE Trans. Power Syst.*, vol. 13, no. 4, pp. 1521–1527, Nov. 1998.

[12] M. S. Chen and W. E. Dillon, "Power system modeling," *Proc. IEEE*, vol. 62, no. 7, pp. 901–915, Jul. 1974.

[13] A. H. El-Abiad and D. C. Tarsi, "Load flow study of untransposed EHV networks," in *Proc. IEEE Power Industry Computer Application (PICA) Conf.*, Pittsburgh, PA, 1967, pp. 337–384.

$$\boldsymbol{Zg_i} = T_{120}^{abc} \begin{bmatrix} z_1 & 0 & 0 \\ 0 & z_2 & 0 \\ 0 & 0 & z_0 \end{bmatrix} T_{abc}^{120} = \frac{1}{3} \begin{bmatrix} z_0 + z_1 + z_2 & z_0 + az_1 + a^2 z_2 & z_0 + a^2 z_1 + az_2 \\ z_0 + a^2 z_1 + az_2 & z_0 + z_1 + z_2 & z_0 + az_1 + a^2 z_2 \\ z_0 + az_1 + a^2 z_2 & z_0 + a^2 z_1 + az_2 & z_0 + z_1 + z_2 \end{bmatrix} \tag{31}$$

[14] R. G. Wasley and M. A. Shlash, "Newton-Raphson algorithm for three phase load flow," *Proc. Inst. Elect. Eng.*, vol. 121, no. 7, pp. 631–638, 1974.
[15] K. A. Birt, J. J. Graf, J. D. McDonald, and A. H. El-Abiad, "Three phase power flow program," *IEEE Trans. Power App. Syst.*, vol. PAS-95, no. 1, pp. 59–65, 1976.
[16] J. Arrillaga and B. J. Harker, "Fast-decoupled three-phase load flow," *Proc. Inst. Elect. Eng.*, vol. 125, no. 8, pp. 734–740, 1978.
[17] M. A. Laughton and A. O. M. Saleh, "Unified phase coordinate load flow and fault analysis of polyphase networks," *Int. J. Elect. Power and Energy Syst.*, vol. 2, no. 4, pp. 181–192, 1980.
[18] B. K. Chen, M. S. Chen, R. R. Shoults, and C. C. Liang, "Hybrid three phase load flow," *Proc. Inst. Elect. Eng.*, pt. C, vol. 137, no. 3, pp. 177–185, 1990.
[19] X.-P. Zhang and H. Chen, "Asymmetrical three-phase load flow study based on symmetrical component theory," *Proc. Inst. Elect. Eng. Gener., Transm., Distrib.*, vol. 143, no. 3, pp. 248–252, 1994.
[20] X.-P. Zhang, "Fast three phase load flow methods," *IEEE Trans. Power Syst.*, vol. 11, no. 3, pp. 1547–1554, Aug. 1996.
[21] X.-P. Zhang, E. Handschin, and M. Yao, "Multi-control functional static synchronous compensator (STATCOM) in power system steady state operations," *J. Elect. Power Syst. Res.*, vol. 72, no. 3, pp. 269–278, 2004.
[22] W. F. Tinney, V. Brandvajn, and S. M. Chan, "Sparse vector methods," *IEEE Trans. Power App. Syst.*, vol. PAS-104, no. 2, pp. 295–301, 1985.

Xiao-Ping Zhang (M'95) received the B.Eng., M.Sc., and Ph.D. degrees in electrical engineering from Southeast University, China, in 1988, 1990, 1993, respectively.

Currently, he is a Lecturer in the School of Engineering, University of Warwick, Coventry, U.K. He was with Nanjing Automation Research Institute (NARI), Ministry of Electric Power, China, working on EMS/DMS advanced application software research and development from 1993 to 1998.

Dr. Zhang was an Alexander-von-Humboldt Fellow at the University of Dortmund, Germany.

Ping Ju (M'95) received the B.Eng. and M.Sc. degrees in electrical engineering from Southeast University, China, in 1982 and 1985, respectively. He received the Ph.D. degree in electrical engineering from Zhejiang University, Hangzhou, China, in 1998.

He is currently a Professor of Electrical Engineering in the College of Electrical Engineering, HoHai University, Nanjing, China.

Dr. Ju was an Alexander-von-Humboldt Fellow at the University of Dortmund, Germany.

Edmund Handschin (F'93) received the diploma in electrical engineering from the Swiss Federal Institute of Technology, Zürich, Switzerland, in 1965 and the Ph.D. degree from Imperial College London, U.K., in 1968.

From 1969 to 1974, he was a staff member at Brown Boveri Research Center, Baden, Switzerland. Since 1974, he has been a Professor and Chair of Electrical Energy Systems at the University of Dortmund, Dortmund, Germany.